JACS
JOURNAL OF THE AMERICAN CHEMICAL SOCIETY
Article
pubs.acs.org/JACS

Unreacted PbI_2 as a Double-Edged Sword for Enhancing the Performance of Perovskite Solar Cells

T. Jesper Jacobsson,[*,†,‡] Juan-Pablo Correa-Baena,[‡] Elham Halvani Anaraki,[‡,§] Bertrand Philippe,[∥] Samuel D. Stranks,[⊥,#] Marine E. F. Bouduban,[¶] Wolfgang Tress,[▽] Kurt Schenk,[⊗] Joël Teuscher,[¶] Jacques-E. Moser,[¶] Håkan Rensmo,[∥] and Anders Hagfeldt[*,‡,■]

[†]University of Cambridge, Department of Chemistry, Lensfield Road, Cambridge CB2 1EW, U.K.

[‡]Laboratory for Photomolecular Science, Institute of Chemical Sciences and Engineering, École Polytechnique Fédérale de Lausanne, CH-1015-Lausanne, Switzerland

[§]Department of Materials Engineering, Isfahan university of Technology, Isfahan, 84156-83111, Iran

[∥]Department of Physics and Astronomy, Uppsala University, Box 516, 75120 Uppsala, Sweden

[⊥]Research Laboratory of Electronics, Massachusetts Institute of Technology, 77 Massachusetts Avenue, Cambridge, Massachusetts 02139, United States

[#]Cavendish Laboratory, JJ Thomson Avenue, Cambridge CB3 0HE, U.K.

[¶]Photochemical Dynamics Group, Institute of Chemical Sciences and Engineering, École Polytechnique Fédérale de Lausanne, CH-1015-Lausanne, Switzerland

[▽]Laboratory of Photonics and Interfaces, Institute of Chemical Sciences and Engineering, École Polytechnique Fédérale de Lausanne, CH-1015-Lausanne, Switzerland

[⊗]École Polytechnique Fédérale de Lausanne, CH-1015-Lausanne, Switzerland

[■]Department of Chemistry − Ångström Laboratory, Uppsala University, Box 538, 75121 Uppsala, Sweden

Supporting Information

ABSTRACT: Lead halide perovskites have over the past few years attracted considerable interest as photo absorbers in PV applications with record efficiencies now reaching 22%. It has recently been found that not only the composition but also the precise stoichiometry is important for the device performance. Recent reports have, for example, demonstrated small amount of PbI_2 in the perovskite films to be beneficial for the overall performance of both the standard perovskite, $CH_3NH_3PbI_3$, as well as for the mixed perovskites $(CH_3NH_3)_x(CH(NH_2)_2)_{(1-x)}PbBr_yI_{(3-y)}$. In this work a broad range of characterization techniques including X-ray diffraction (XRD), scanning electron microscopy (SEM), transmission electron microscopy (TEM), photo electron spectroscopy (PES), transient absorption spectroscopy (TAS), UV−vis, electroluminescence (EL), photoluminescence (PL), and confocal PL mapping have been used to further understand the importance of remnant PbI_2 in perovskite solar cells. Our best devices were over 18% efficient, and had in line with previous results a small amount of excess PbI_2. For the PbI_2-deficient samples, the photocurrent dropped, which could be attributed to accumulation of organic species at the grain boundaries, low charge carrier mobility, and decreased electron injection into the TiO_2. The PbI_2-deficient compositions did, however, also have advantages. The record V_{oc} was as high as 1.20 V and was found in PbI_2-deficient samples. This was correlated with high crystal quality, longer charge carrier lifetimes, and high PL yields and was rationalized as a consequence of the dynamics of the perovskite formation. We further found the ion migration to be obstructed in the PbI_2-deficient samples, which decreased the *JV* hysteresis and increased the photostability. PbI_2-deficient synthesis conditions can thus be used to deposit perovskites with excellent crystal quality but with the downside of grain boundaries enriched in organic species, which act as a barrier toward current transport. Exploring ways to tune the synthesis conditions to give the high crystal quality obtained under PbI_2-poor condition while maintaining the favorable grain boundary characteristics obtained under PbI_2-rich conditions would thus be a strategy toward more efficiency devices.

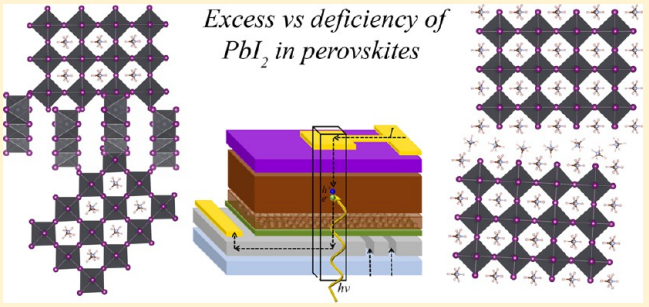

INTRODUCTION

Lead halide perovskites have during the past few years attracted considerable interest as light absorbers in solar cells. The first

Received: June 19, 2016
Published: July 20, 2016

DOI: 10.1021/jacs.6b06320
J. Am. Chem. Soc. 2016, 138, 10331−10343

paper on the matter was published in 2009.[1] After some key advances in the following years[2−6] the field has expanded rapidly with top efficiencies now reaching beyond 22%.[7] There is also a realistic hope of perovskites reaching the market, either as stand-alone cells or as top cells in tandem configurations with conventional solar cells.[8−10]

The standard perovskite in the community has so far been methylammonium lead iodide, $MAPbI_3$, but both the organic ion and the halide can be substituted. MA has for example been replaced with formamidinium (FA),[11−14] and iodine by chlorine[15] and bromine.[16] The MA/FA and Br/I ratios can also be changed simultaneously,[14,17,18] and the best cells at the moment are based on mixed perovskites with compositions around $MA_{1/3}FA_{2/3}Pb(Br_{1/6}I_{5/6})_3$.[19,20]

For a given perovskite, the precise stoichiometry is important as well. Most notably, a slight excess of PbI_2 in the perovskite film has been observed to be beneficial.[19,21,22] The best performing cells have a few percent excess PbI_2 in them but exactly why is still unclear. This bring us to the core of this paper, which aims at investigating how an excess, or a deficiency, of PbI_2 affect the physics and the performance of mixed perovskite devices.

The possible benefit of excess PbI_2 was first reported in studies using two-step synthesis methods.[22,23] A PbI_2 film is then being deposited and subsequently exposed to solutions of the organic salts whereupon the perovskite forms.[23,24] The overall stoichiometry depends on the length of the second step. Short times results in uncompleted conversion and some PbI_2 will consequently remain in the final film.[23,25,26] Due to trivial geometry, PbI_2 will to a greater extent be found close to the back contact. A thick PbI_2 layer between the back contact and the perovskite results in electronic insulation and poor cell performance.[25−27] The highest cell efficiencies were, however, obtained when most but not all of the PbI_2 was converted into the perovskite.[26] For exposure and subsequent annealing times slightly longer than required for complete conversion, the perovskite begins to degrade into PbI_2 and a volatile organic component.[28] This PbI_2, formed as a consequence of perovskite degradation, could also be beneficial.[29,30] Even longer reaction times result in severe and detrimental degradation and a fine balance is to be found.

One-step methods, which we use in this study, provide a higher degree of control of the stoichiometry and give consistent results indicating that small amounts of PbI_2 in the deposited films are beneficial for device performance.[19,21] Not everyone has, however, found the excess PbI_2 to be beneficial,[25,31,32] though those results appear to be exceptions.

The reason behind this observation, the mechanistic details, and whether or not PbI_2 is truly essential for high efficiency devices or merely the cause of favorable secondary effects, achievable by other approaches, are still open questions.

A few hypotheses focus on energy level alignment. PbI_2 may for example passivate the TiO_2 interface[19,26,29,33] and thereby decrease hole recombination, either due to surface passivation or band edge matching between TiO_2, PbI_2, and the perovskite (Figure 1a). Another hypothesis is that PbI_2 could facilitate electron injection into TiO_2.[21,34] As an excess of PbI_2 are beneficial also when blocking layers other than TiO_2 are used, i.e., SnO_2,[17] those appear to be less likely explanations. At the perovskite/HTL interface PbI_2 could, according to a similar reasoning, act as an electron blocking layer, facilitate hole injection, and thereby decrease recombination[29,35] (Figure 1b). If the PbI_2 layers are too thick, or if the energy matching is wrong, they may instead insulate individual grain and block charge transfer (Figure 1c,d).

Another set of hypotheses focuses on grain boundaries. The composition of the center of the perovskite grains could possibly be fairly insensitive toward small changes in overall stoichiometry. The grain boundaries and the regions between the grains would thus by necessity be highly sensitive to the overall composition (Figure 1e−g). This could affect, for example, defect states, dangling bonds, conductivity, doping, and ion migration.

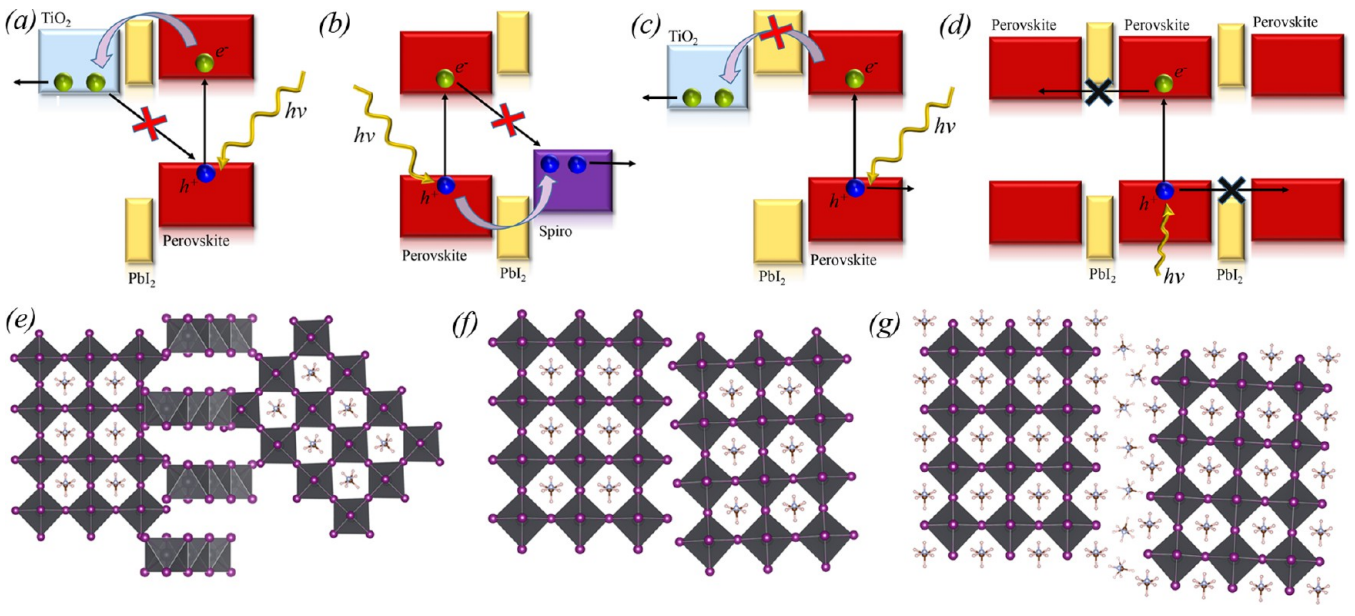

Figure 1. Consequences of PbI_2 in the perovskite film related to possible energy alinements suggested in the literature and an artistic illustration of difference grain boundary character as a function of overall stoichiometry. (a) PbI_2 as a passivating layer at the back contact. (b) PbI_2 as a passivation layer next to the hole-selective layer. (c) PbI_2 as an electron blocking layer next to the back contact. (d) PbI_2 as charge carrier barrier between perovskite grains. (e) Grain boundary with a large surplus of PbI_2. (f) Grain boundary with a small deficiency of organic species. (g) Grain boundary with a large surplus of organic species.

DOI: 10.1021/jacs.6b06320
J. Am. Chem. Soc. 2016, 138, 10331−10343

Some results indicate recombination to be faster within grain boundaries deficient in PbI_2.[29,36] PbI_2 would thus act as a passivation layer between the grains.[36] This is supported by computations that indicate that PbI_2-rich conditions results in good termination with fewer intra band gap states as possible recombination centers.[37] Other computations show that the conditions under which the perovskite is formed influences the type and the number of defects within the perovskite[38] and that synthesis under iodine poor conditions leads to less bulk defects related to deep traps. Those conclusions are not directly generalizable to the role of PbI_2 in perovskite films, but as they show a correlation between formation of bulk defect and synthesis conditions, this may be important. The general view is that the perovskite grain boundaries are defect tolerant and intrinsically benign, which is supported by theoretical simulations,[39] and there are claims that charge transport is especially efficient in the grain boundaries.[40] This may, however, change as a function of the composition of the grain boundaries.

Finally, there are hypotheses stating that PbI_2 is not beneficial in itself, but rather are correlated with other secondary advantageous effects. That could for example be larger perovskite grains[19,21] or improved crystallinity.[21] Remnant PbI_2 may thus be a redundant component as those benefits may be engineered along other paths as well.

A deeper understanding of the interplay between PbI_2, overall stoichiometry, and device performance would be valuable for further solar cell development. In this paper, we do not reach complete understanding, but we present the most comprehensive investigation up to date on the topic, which takes us closer. Here we discuss the aggregated results from a wide range of techniques used to investigate perovskites with compositions that stretches from a large deficiency of PbI_2 (henceforth referred to as understoichiometric) to a large surplus of PbI_2 (henceforth referred to as overstoichiometric). The results illuminate connections between device performance, stoichiometry, ion movement, recombination behavior, and trap formation valuable for future work toward improving perovskite devices.

EXPERIMENTAL METHODS

The perovskite solar cells were prepared in line with previous reports.[17,19,20,41−49] The solar cell stack is composed of FTO, a compact TiO_2-layer, mesoporous TiO_2, a mixed perovskite deposited by spin coating using a one-step antisolvent method, doped Spiro-MeOTAD as a hole conductor, and an evaporated gold contact. A detailed description of the synthesis is found in the Supporting Information. Unique for this sample series is the variation in stoichiometry. All the final precursor solutions had the following concentrations: [Pb2+] = 1.25 M, [$PbBr_2$] = 0.22 M, [PbI_2] = 1.04 M, [MABr] = [$PbBr_2$] = 0.22 M. To probe the importance of PbI_2, [FAI] was varied. When we henceforth state a composition as +10% with respect to PbI_2 we mean that [FAI] = [PbI_2]·0.9. Analogously, we by −10% mean that [FAI] = [PbI_2]·1.1. Plus 10% thus mean a surplus of PbI_2 in the solution (or a deficiency of FA), which result in excess PbI_2 in the perovskite films.

Perovskites with different stoichiometry where investigated by XRD, SEM, TEM, UV−vis spectroscopy, steady state photoluminescence (PL), transient absorption spectroscopy (TAS), confocal PL mapping, Photoelectron spectroscopy (PES), Hard X-ray PES (HAXPES), Soft X-ray PES (SOXPES). Complete devices were characterized in terms of *JV* characteristics, external photocurrent efficiency (EQE) and electroluminescence. The details concerning the equipment and the experimental parameters are found in the Supporting Information.

RESULTS

Basic Optical and Crystallographic Characterization. X-ray diffraction was measured on a subset of the samples with varying stoichiometry (Figure 2a) stretching from

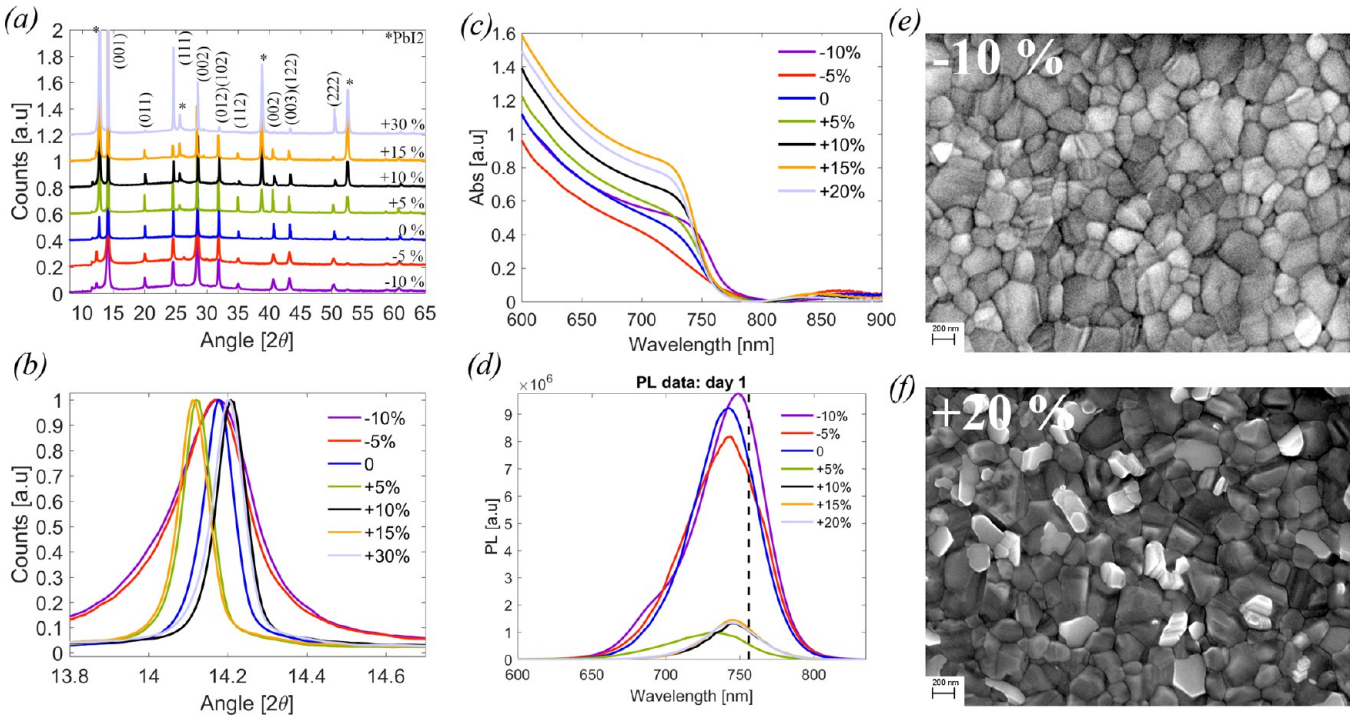

Figure 2. (a) XRD data normalized with respect to the strongest perovskite reflex (001) for seven different stoichiometries. Data are shifted in height to be easier to compare. The full set of diffraction figures are given in the SI (b) The (001) peak of the normalized data in (a). (c) UV−vis for the same samples as in (a). (d) PL data for the same samples measured at the day of deposition. (e) and (f) Top view SEM images for a PbI_2-deficient and a PbI_2-rich sample. The scale bars are 200 nm. The full set of SEM images are found in the SI.

DOI: 10.1021/jacs.6b06320
J. Am. Chem. Soc. 2016, 138, 10331−10343

−10% understoichiometric (PbI_2-deficient) to 20% overstoichiometric (PbI_2-rich). One single crystalline perovskite phase formed in all samples. By comparing normalized diffraction data for the (001)-reflection (Figure 2b), no systematic peak shifts were observed, which show the composition of the crystalline perovskite to be unaffected by the overall stoichiometry. A small random shift is seen, which indicates a slight shift in the I/Br ratio.[20] On the basis of previous quantifications, the observed shifts are too small to be of significant importance for the device performance.[20] The symmetry of the perovskite phase was found to be cubic, as expected based on previous measurements[20,45] and theoretical considerations.[50]

The diffraction peak in Figure 2b is wider for the two understoichiometric samples, which indicates smaller crystallites. By Scherrer's equation we estimate those to be around 30 nm for the understoichiometric samples and 100 nm or more for the rest. A feature size of 30 nm does, however, not correlate with the SEM data (Figure 2e,f) discussed below where the grains appears to be a few hundred nm, and thus might consist of several crystallites.

Apart from the perovskite, the only crystalline phase observed is PbI_2, which, as expected, increases in amount for the more overstoichiometric samples. The PbI_2-peaks are rather narrow. The PbI_2 in the films are thus either amorphous or in the form of rather large crystallites, i.e., more than 100 nm.

UV−vis absorption was measured on the same subset of samples (Figure 2c). The overall absorption behavior was rather unaffected by stoichiometry and had a low background signal indicating uniform films of high quality with respect to macroscopic inhomogeneity. There appears to be a difference in absolute absorption between the samples. However, this was caused by a measurement artifact and the effect disappeared in control measurements using an integrating sphere (SI).

The band gaps were extracted from the absorption data, as elaborated in the Supporting Information,[51−53] and were found to be between 1.62 and 1.65 eV. Valence band spectroscopy was also used and reveled no dependence in the valence band edge position with respect to the stoichiometry (SI).

PL was measured both on the day of deposition and after 30 days of storage in dry air. Directly after deposition, one single strong peak was observed in all samples (Figure 2d). The peaks were centered close to the band gap energy, with the exception of a slight blue shift in the +5% sample. The PL and the absorption data thus supports the conclusion form the XRD data that the perovskite phase essentially is the same in the different samples.

The PL intensities were higher for the stoichiometric and the understoichiometric samples. At the day of synthesis, the difference was up to 1 order of magnitude (Figure 2d). The difference hade some batch dependence, indicating that competing mechanisms are involved in determining the emissivity. After a month in dry air, the difference in intensity decreased moderately (SI). Large difference in PL intensity have been reported in the literature and have been reported to different defects and there quenching,[54] suggesting either less defects or efficient blocking of them in the PbI_2-poor samples.

Under strong illumination (10 sun), the dominant peak in the overstoichiometric films began to broaden and split into two peaks (SI). The new peaks were located at lower energies, consistent with formation of an iodine-enriched phase. Such a secondary phase can already in small quantities act as efficient recombination centers detrimental for device performance.[20] This was not observed in the understoichiometric samples, indicating higher photo stability. On the basis of *JV* hysteresis for the corresponding devices, we relate this effect to differences in ion migration, which appears to be slower over PbI_2-deficient grain boundaries. This photoinduced ion migration is discussed in more detail in a parallel paper.[55]

SEM was used to further investigate the grain size and the surface morphology, which are known to influence the device performance.[19,43,56] Cross section images showed the film thickness to be rather unaffected by the stoichiometry (SI). Examples of top view SEM images are found in Figure 2e,f. A complete set of images are found in the Supporting Information. The surface morphology was rather smooth and the pin holes were few for all samples. The overstoichiometric films were slightly rougher, but we have not quantified this.

In terms of grain size, the cross section images are consistent with the top views. A typical grain size is in the order of 200 nm for all samples, but possibly slightly smaller around the stoichiometric composition. The grain size is smaller than the cross section of the perovskite film. A large fraction of the photo generated charge carriers thus has to pass one or more grain boundaries before collection.

A grain size of 200 nm is inconsistent with the XRD data for the understoichiometric samples. This possibly means that the grains observed in the SEM images are monocrystalline for the overstoichiometric samples but polycrystalline in the understoichiometric ones. This could possibly correlate with the striations observed on the grains in the understoichiometric samples (Figure 2e), which could be a proxy for planar defects and a change in the stacking direction within the grains. This indicates that a difference in device performance more likely are an effect of crystal quality, stacking within individual grains, polycrystallinity of grains, and the property of the grain boundaries rather than due to the average size of the perovskite grains per se.

Photoelectron Spectroscopy. If the composition of the perovskite phase is essentially unaffected by overall stoichiometry, the grain boundaries will according to the mass balance be more dependent. The most accessible grain boundaries are located at the surface. Although possibly different from the internal grain boundaries, they provide an indication of what to expect based on the overall stoichiometry.

As a baseline for further comparison, reference spectra were measured for $FAPbI_3$, $MAPbBr_3$, and $FA_{0.85}MA_{0.15}PbBr_{0.45}I_2$ (Figure 3a). The I 4d core levels (53−48 eV), and the Pb 5d core level (25−15 eV) are all in line with previous results found in the 80−0 eV range.[57] So is also the Br 3d core level (72−67 eV) (Figure 3b). Those signals thus originate from a similar probing depth, which means that the peak intensities easily can be linked to the composition via atomic cross sections. Since the analysis only includes d-orbitals, the quantification is also rather insensitive to factors linked to the sample, the detector, and the X-ray polarization configuration.

The spectra were intensity normalized with respect to the Pb 5d5/2 peak. For $FA_{0.85}MA_{0.15}PbBr_{0.45}I_{2.55}$, the experimental Br/Pb and I/Pb ratio was 0.45 and 2.36 respectively. The theoretical values based on the bulk stoichiometry are 0.45 and 2.55. The I/Pb ratio for $FAPbI_3$ was estimated to be 2.4 and the Br/Pb ratio in $MAPbBr_3$ to 2.93 (instead of 3 theoretically). The presence of PbI_2 at the probing depth decreases the I/Pb ratio and explains the difference between the experimental and theoretical values. Worth to mention is that those values indicate that pure stoichiometric $MAPbBr_3$ more easily is formed than $FAPbI_3$, which contains more PbI_2 at the surface.

The MA and FA features can easily be distinguished from each other by the N 1s spectra (Figure 3c). $FAPbI_3$ and $MAPbBr_3$ give

DOI: 10.1021/jacs.6b06320
J. Am. Chem. Soc. 2016, 138, 10331−10343

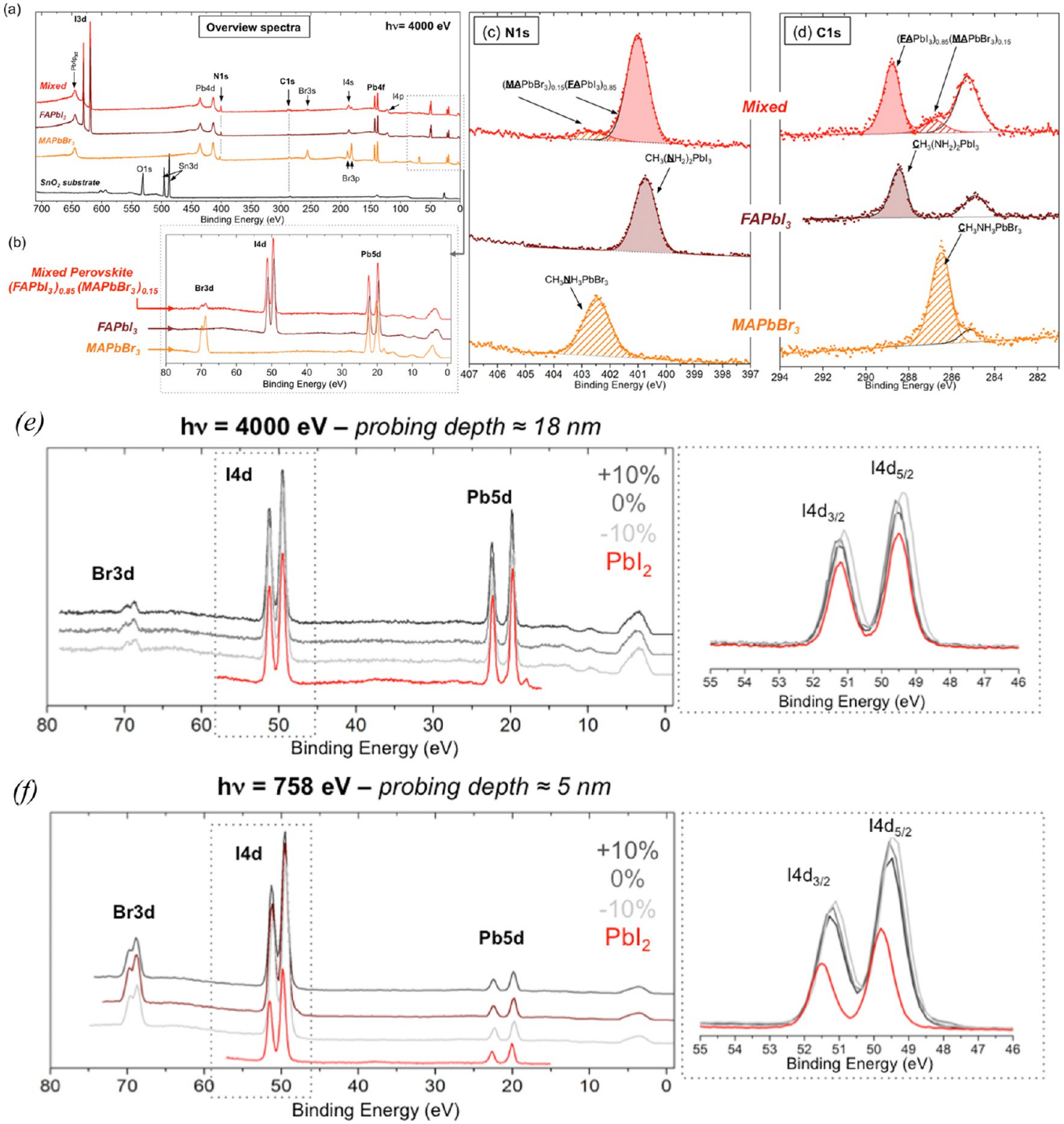

Figure 3. (a) Overview spectra of the mixed perovskite (stoichiometric, i.e., 0), $FAPbI_3$ and $MAPbBr_3$ deposited on amorphous SnO_2/FTO and of the bare amorphous SnO_2/FTO substrate recorded with a photon energy of 4000 eV (in red, brown, orange, and black respectively). The SnO_2 substrate was normalized with respect to intensity vs Sn $3d_{5/2}$. No substrate peaks were observed in the perovskite spectra, demonstrating full coverage. (b) Br 3d/I 4d/Pb 5d (c) N 1s and (d) C 1s core level spectra of the mixed perovskite, $FAPbI_3$ and $MAPbBr_3$. (e) and (f) Br 3d/I 4d/Pb 5d core level peaks of the perovskite materials with three different stoichiometries: −10%, 0, +10% in light gray, gray, and dark gray respectively recorded at 4000 eV (e) and 758 eV (f). All the spectra were intensity normalized to the Pb $5d_{5/2}$ core level peaks. A zoom on the I 4d peak is shown on the right. The spectra of the PbI_2 precursors are shown as reference (in red).

a single peak located at ∼400.8 and ∼402.5 eV respectively. Both peaks are found and are separable in the mixed perovskite, although at slightly higher energy (∼401.0 and ∼402.7 eV). The ratio between the metal and the halides can be determined based on Figure 3b and the N 1s signal can be used to estimate the cation ratio. For the mixed perovskite, MA:FA was estimated to 12:88, which is relatively close to the overall experimental composition of 15:85. Quite similar information is given by the C 1s spectra where $FAPbI_3$ and $MAPbBr_3$ has a specific peak at ∼288.4 and ∼286.5 eV (Figure 3d). A third peak is observed at 285.2 eV, which is attributed to common surface contaminations usually found on ex situ prepared samples. This peak can overlap

DOI: 10.1021/jacs.6b06320
J. Am. Chem. Soc. 2016, 138, 10331−10343

with the MA and FA signal (see SI) and the Cs1 signal was therefore not used for quantifications.

PES-spectra in the energy range of 80−0 eV for three different stoichiometries (−10%, 0, + 10%) of the mixed perovskite, $FA_{0.85}MA_{0.15}PbBr_{0.45}I_{2.55}$, are found in Figure 3e,f. Three different photon energies were used in order to vary the probing depth, 758, 2100, and 4000 eV. Using values from Tanuma et al.,[58] a probing depth of approximately 18 nm are explored with photon energies of 4000 eV (HAXPES). A higher surface sensitivity with a probing depth of around 5 nm is achieved with a photon energy of 758 eV (SOXPES). At the intermediate energy of 2100 eV, the probing depth was estimated to ∼11 nm. The probing depths are reasonable estimates but the exact values depend on details in the material structure.

By normalizing the spectra with respect to the lead component, the variation and difference in the iodine peak can be compared. At the highest probing depth (4000 eV, ∼ 18 nm), the peak intensity of I 4d clearly is, as expected, different between the perovskites and PbI_2. A difference between the three samples is visible indicating some stoichiometric difference between them. At $h\nu$ = 758 eV, which represent a smaller probing depth, the same differences can be observed between the samples and a larger change can be observed when compared to PbI_2. On the basis of these spectra, Table 1 presents the calculated I/Pb (a), Br/Pb (b), and I/Br (c) ratio estimated with three different photon energies for the three different mixed perovskite materials. PbI_2 is included as a reference and to validate our quantifications.

Table 1. Intensity Ratios between Different Core Levels Calculated from Experimental Results[a]

(a) I/Pb intensity ratio					
$h\nu$ [eV]	probing depth [nm]	−10%	0	+10%	PbI_2
4000	18	2.49	2.36	2.28	1.96
2100	11	3.35	3.08	2.90	–
758	5	4.36	4.22	3.82	2.03
(b) Br/Pb intensity ratio *(theo. 0.45)*					
$h\nu$ [eV]	probing depth [nm]	−10%	0	+10%	PbI_2
4000	18	0.39	0.45	0.45	–
2100	11	0.50	0.51	0.53	–
758	5	0.83	1.00	0.80	–
(c) I/Br intensity ratio *(theo. 5.66)*					
$h\nu$ [eV]	probing depth [nm]	−10%	0	+10%	PbI_2
4000	18	6.38	5.25	5.08	–
2100	11	6.74	6.06	5.51	–
758	5	5.24	4.19	4.77	–

[a](a) I/Pb, (b) Br/Pb, and (c) I/Br of the mixed perovskites with three different stoichiometry as function of the excitation energy (4000, 2100, and 758 eV). The I/Pb ratio of PbI_2 is also given. The relative atomic percentage of Pb, I, and Br are presented in the SI.

The estimated I/Pb ratio is given in Table 1a. The I/Pb ratio for PbI_2 is close to 2 in agreement with its chemical formula. For the deepest probing depth (4000 eV, ∼18 nm), the experimental values for the mixed perovskite are below 2.55, which is the theoretical value, and decreases from the −10% to the +10% stoichiometry. This is in line with more unreacted PbI_2 in the films as is expected based on the stoichiometry of the precursor solutions. Also the PbI_2-deficient sample (−10%) has a ratio below 2.55 suggesting noncomplete conversion into the perovskite, in line with the XRD data. For the more surface sensitive technique (758 eV, ∼5 nm), the I/Pb ratios are higher than 2.55. This indicate unreacted FAI in the surface layer. The I/Pb ratio is still decreasing from −10% to +10%, with the highest value for the PbI_2-deficient sample, which consequently has a relative excess of FAI.

Those data are consistent with a model of perovskite growth that starts with precipitation of PbI_2 followed by intercalation of the organic ions under the formation of the perovskite. This is opposed to a single step growth of the perovskite. The perovskite would then grow from the outside−in, which preferably will leave unreacted organic species at the surface rather than PbI_2, which preferentially would be found deeper down in the grains if the conversion is not complete.

The Br/Pb ratio (Table 1b) does not show any clear trend with respect to stoichiometry. This agrees with the observation that $PbBr_2$ more easily forms the perovskite, which should make the Br/Pb ratio less sensitive to the amount of PbI_2 in the system. When the probing depth decreases, an increase is observed but not as significant as for the I/Pb ratio. This either indicates a slight bromide enrichment in the surface perovskite, or the presence of unreacted bromide salts on the surface but at a lower amount than the iodide salts.

The I/Br ratio (Table 1c) confirm the point raised earlier. The I/Br ratio decreases from −10% to +10% in line with the excess of FAI, especially when the synthesis is deficient in PbI_2. When the probing depth is decreased, the I/Br ratio decreases slightly in agreement with a surface with a more bromide rich perovskite phase.

The FA/MA ratio for the different stoichiometries was determined based on the N 1s core level spectra at 4000 and 758 eV (Figure 4). No significant changes were observed between the three samples or when the analysis depth was changed and FA was always representing between 85 and 90% of the total amount of cations. This stability may be surprising considering the fluctuation observed in Table 1. However, we have seen that at the surface, the slight diminution of $FAPbI_3$ is balanced by the presence of FAI, which will keep the FA/MA ratio relatively constant. The main difference observed at the surface of the perovskite samples with different stoichiometries are schematically summarized in Figure 5.

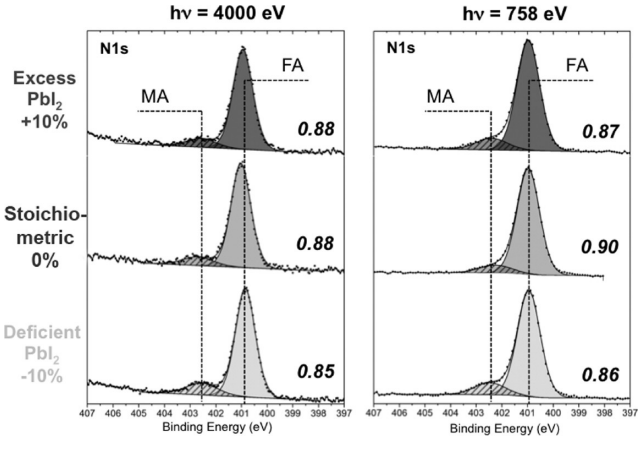

Figure 4. N 1s core level peaks of the perovskite materials with three different stoichiometries: −10%, 0, +10% in light gray, gray and dark gray respectively recorded at 4000 eV (left) and 758 eV (right). The proportion of FA is indicated on each spectrum.

The PES measurements confirm that the perovskite phase is rather unaffected by the stoichiometry, they demonstrate a surplus of organic species at the surface dependent on the

DOI: 10.1021/jacs.6b06320
J. Am. Chem. Soc. 2016, 138, 10331−10343

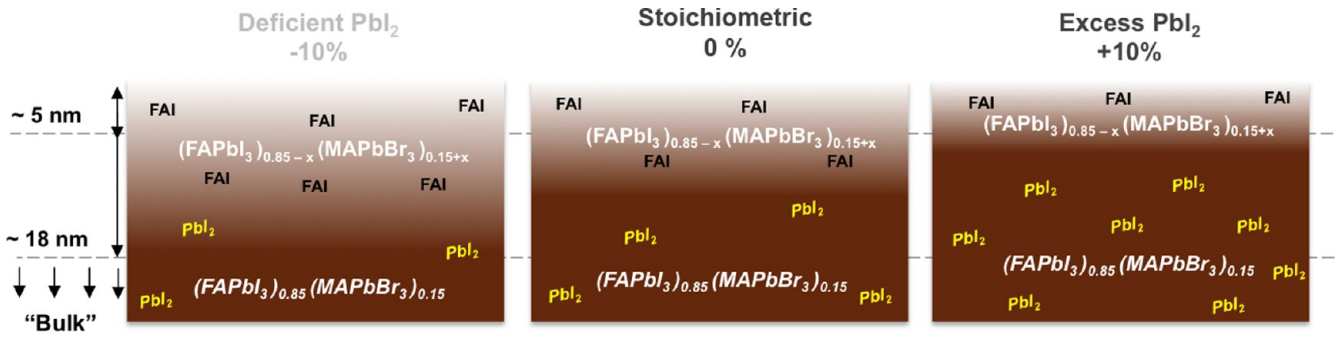

Figure 5. Schematic illustration summarizing the main difference observed by PES between the three different stoichiometries: −10%, 0, and +10%.

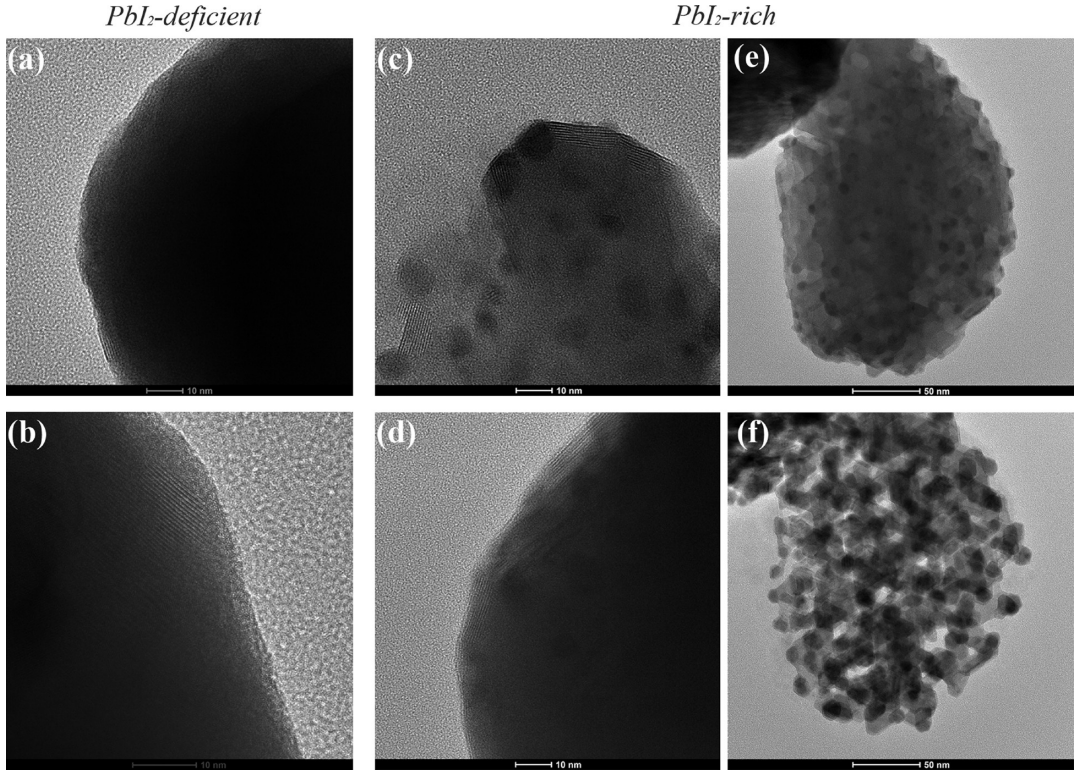

Figure 6. (a,b). TEM images of a PbI_2-deficient sample. (c–f). TEM images of a PbI_2-rich sample. (e) and (f) is an image of the same spot illustrating sample degradation under the electron beam. The samples were prepared by scratching of a perovskite film deposited on SLG with a razor blade, in which the TEM-grid then was rubbed.

stoichiometry, and that unreacted PbI_2 is located within the perovskite film.

TEM. Samples of over and understoichiometric perovskites were investigated by TEM to get more direct information about the grain boundaries. Much of the sample was too thick to be electron transparent but some grains of a suitable size could be found. For the high resolution images in Figure 6a–d, lattice fringes, which indicate a high degree of crystallinity, are seen for both the under- and overstoichiometric sample. Those appear to stretch out to the surface of the grains to a larger degree in the samples with more PbI_2 (compare Figure 6b and 6d). That would support the grain boundary hypothesis presented based on the PES data. We must stress that this not is a solid conclusion but rather a weak indication in line with the other data. The reason for this ambiguity is sample instability. At high magnifications, the surface of the grains sometimes appears to melt and shrink, making it difficult to distinguish real structural effects from beam induced artifacts. An example of the beam damage is given by comparing Figure 6e,f where the same spot is photographed after different exposure times.

The beam induced degradation are affected by the stoichiometry. In the overstoichiometric sample, dark grains a few nm across are seen (Figure 6c and 6e), which gets more pronounced with longer exposure times (Figure 6f). This was not observed to the same extent in the understoichiometric sample. Those grains are likely PbI_2. The higher frequency of these dots in the overstoichiometric sample and the uniform distribution indicates that not all unreacted PbI_2 is located at the grain boundary but it also is distributed, in amorphous form, within the particles. This is in line with the PES-results and points toward a crystallization process where the perovskite grains are grown from the outside of PbI_2-grains by diffusion and intercalation of the organic ions. A surplus of organic ions would facilitate complete conversion whereas a deficiency of organic ion may leave small pockets of unreacted amorphous PbI_2 within the perovskite grains. This would further indicate a higher crystal

DOI: 10.1021/jacs.6b06320
J. Am. Chem. Soc. 2016, 138, 10331–10343

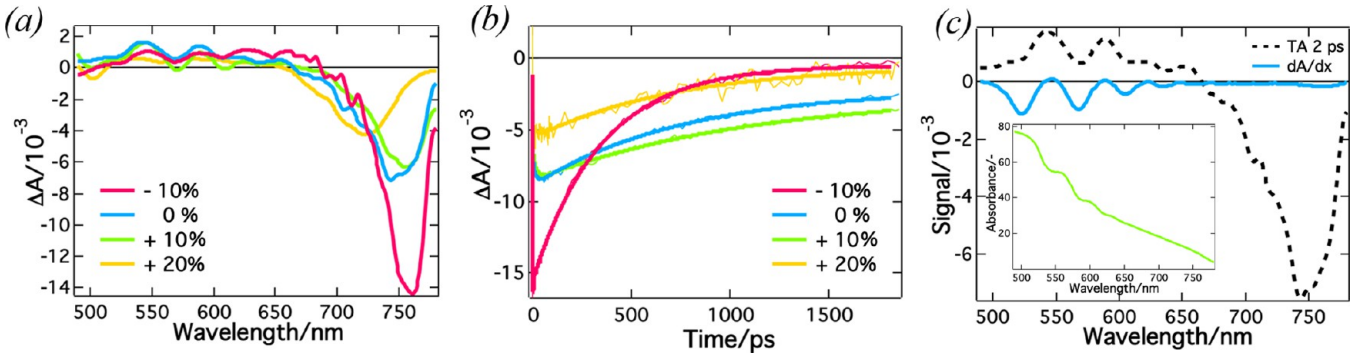

Figure 7. (a) Transient absorbance spectra (smoothed) of four different stoichiometries: -10%, 0%, 10%, and 20%. Measured at 2 ps after excitation with a 480 nm laser. Data is normalized with respect to the absorbance at 480 nm. (b) Transient absorbance dynamics after 480 nm excitation, measured at the maximum of the ground state bleaching in (a), which are 760, 750, 756 and 723 nm for the −10%, 0%, 10% and 20% sample, respectively. Thin lines are raw data and bold lines are multiexponential fits. (c) Modeled electro-absorption (first derivative of the absorption spectrum, blue line) for the samples with 10% excess PbI_2 superimposed on the smoothed transient absorbance spectrum at 2 ps (dashed black line). The inset is the absorbance as a function of wavelength for the same film.

core quality in the PbI_2-deficient samples but with less well-defined grain boundaries. This is in line with a high V_{oc} and poor transport properties discussed below.

Within the bigger perovskite grains, these small inclusions could act as seeds that under stress accelerate the decomposition of the perovskite into PbI_2 and organic salts, explaining the higher stability observed in the understoichiometric sample.

Transient Absorption Measurements. To access the time dynamics of the photoexcited states, transient absorption spectroscopy (TAS) was carried out on perovskite films of four different stoichiometries: −10%, 0%, +10%, and +20%.

The dominant feature of the TAS spectra measured at 2 ps after a 480 nm excitation pulse (Figure 7a) was a negative signal with a maximum amplitude around 760 nm. This was assigned to a combination of ground-state bleaching (GSB) and stimulated emission (SE).[59−62] The maximum was observed to shift from 760 nm for the understoichiometric sample to 723 nm for the most overstoichiometric sample. Such a blue shift is consistent with a slightly more bromide rich composition but could also be related to differences in the strain or in the tilt of the PbI_2-octahedra, which is known to influence the optical properties.[50,63−65]

The spectral features also broaden as one moves toward the most overstoichiometric sample. Both the spectral shift and the broadening indicate a more complex material with potentially more strain and compositional inhomogeneity. That does not correlate with lower device performance as seen below, but a narrower bleach peak could possibly be associated with a higher crystal core quality and a higher $V_{oc.}$ We finally wish to stress the appearance of a distinct spectral signature (negative at 500 nm) in the overstoichiometric samples (+20%), which we attribute to PbI_2.

The time-dependent behavior of the GSB+SE signal was obtained by extracting the time dynamics at its respective maxima (Figure 7b). The time traces were fitted with a triexponential model convoluted with a Gaussian instrument response function. The resulting time constants: τ_1, τ_2, and τ_3 are provided in Table 2. τ_1 describes the rise of the transient, τ_2 denotes the recovery of the GSB+SE signal, and τ_3 is associated with long-lived species.

On the contrary to τ_1 and τ_3, the second time constant, τ_2, shows a clear trend with the stoichiometry and increases with increasing PbI_2-content and range from 0.91 ps for the most understoichiometric sample to 24 ps for the PbI_2-richest sample. The exact mechanism for the difference in the GSB+SE signal

Table 2. Fitting Constants Extracted from a Tri-exponential Function Convoluted with a Gaussian IRF with a FWHM = 80 fs

sample	$\Lambda_{max\ [nm]}$	τ_1 [ps]	τ_2 [ps]	τ_3 [ps]
−10%	760	0.39	0.91	348
0%	750	0.29	13	762
10%	756	0.31	17	1105
20%	723	0.20	24	723

recovery is at this stage hard to pinpoint, and those decay times should not be confused with the charge carrier lifetimes under solar illumination, which are substantially longer.

Another interesting feature is the presence of oscillations between 500 and 700 nm in the transient absorption spectra (Figure 7a). As emerges from Figure 7c, featuring the 2 ps TA-spectra for one of the overstoichiometric samples (10%) superimposed to a modeled electro-absorption signal, those oscillations match the spectrum of a short-lived photoinduced electro-absorption signal. The presence of such a signal is interesting as it is indicative of the presence of photoinduced carriers exhibiting a permanent dipole and yielding a sensible electric field. At the moment we attribute this to the presence of PbI_2-domains within the materials.

Time-Resolved PL Mapping. To further understand the recombination kinetics, confocal PL maps of samples with different stoichiometries were sampled. PL measurements give a relative measure of the fraction of radiative and nonradiative decay and to achieve the highest device performance, nonradiative decay should be minimized or eliminated.[66] To ensure morphologies comparable to other studies while avoiding significant quenching of the PL signal from electron injection, the mesoporous TiO_2 scaffold was coated with a conformal 5 nm thick layer of insulating Al_2O_3 by ALD, on top of which the perovskites were deposited. Confocal PL intensity maps with excitation through the glass are given in Figure 8a−d and the corresponding intensity histograms in Figure 8e. The understoichiometric sample (−10%) shows the most uniform emission distribution and the absolute intensity is almost an order of magnitude higher than for the other compositions, consistent with the PL data in Figure 2d. The other compositions have similar net intensity magnitudes, though we note that the +10% composition appears to have two different distributions of intensity of emitting species and a lot of heterogeneity in the emission. The time-resolved PL decay (Figure 8f) when exited through the

DOI: 10.1021/jacs.6b06320
J. Am. Chem. Soc. 2016, 138, 10331−10343

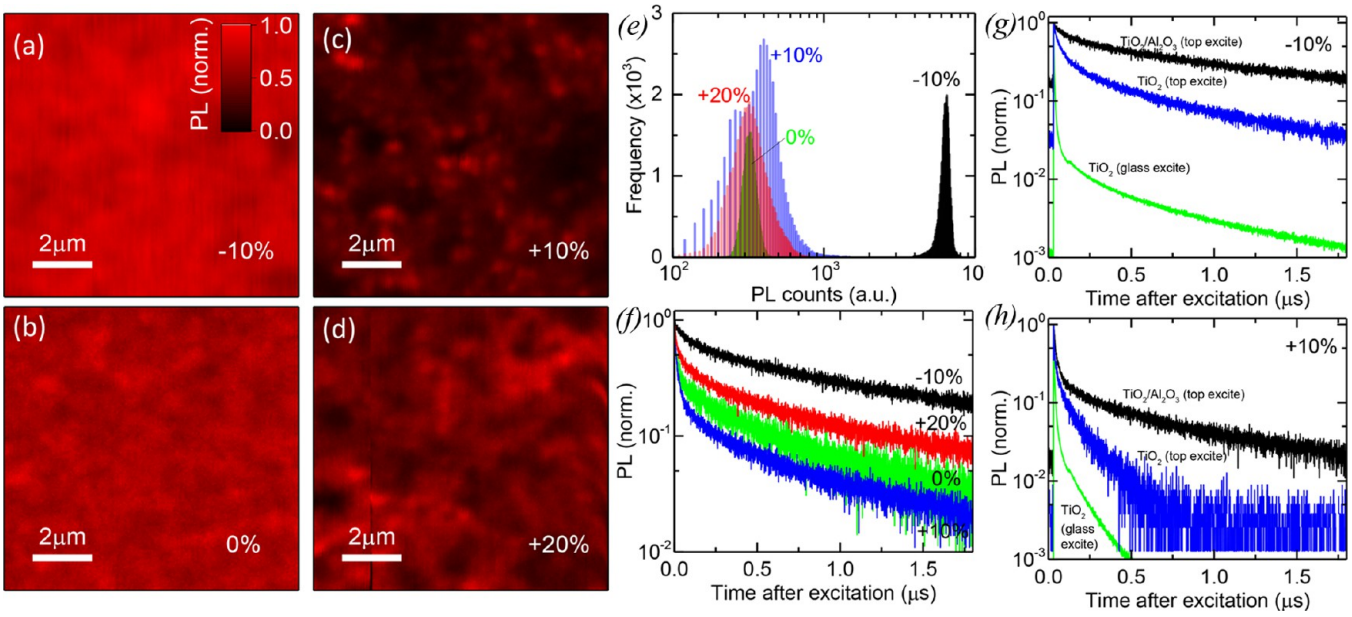

Figure 8. Confocal photoluminescence (PL) intensity maps of the (a) −10%, (b) 0%, (c) +10%, (d) +20% configurations infiltrated into a non-quenching mesoporous scaffold and measured through the glass side. The maps were normalized to their peak value. (e) Histograms of the absolute intensities extracted from the PL maps. (f) Time-resolved PL decays of the samples when excited through the top side with the same laser settings as above. (g,h). Time-resolved PL measurements for the (g) −10% and (h) +10% compositions when exciting the noninjecting (TiO_2/Al_2O_3) sample from the top-side (black) or the injecting sample (TiO_2) from either the top-side (blue) or the glass-side (green). Samples were photoexcited with a 405 nm laser with a repetition rate of 0.5 MHz and a fluence of 2 $\mu J/cm^2$/pulse.

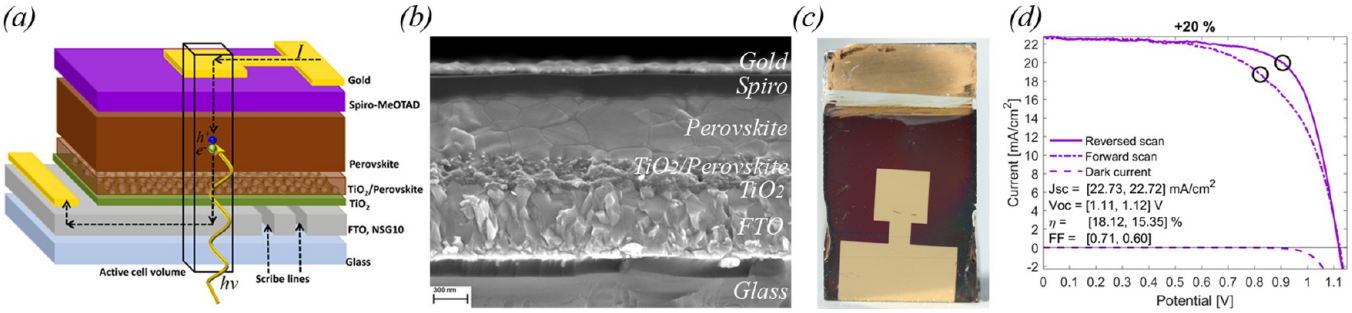

Figure 9. (a) An illustration of the device architecture. (b) A cross section SEM image of a typical device (+15%). The scale bar is 300 nm. (c) A photo of a devices. (d) *JV* data for one of the best devices. The full set of *JV* curves are given in the Supporting Information.

top-side gives an idea of the average lifetimes. These reflect the intensity distributions where the longest lifetime is seen for the understoichiometric sample (−10%). This suggests that the highest V_{oc} may be found for the understoichiometric compositions.

To investigate how well the PL is quenched from electron injection into the mesoporous TiO_2, measurements were performed on samples without the insulating Al_2O_3-interlayer. For simplicity, only the −10% and +10% compositions are compared (Figure 8g,h). When excited through the top side, most of the charge carriers are generated far from the injection electrode. For the understoichiometric sample (−10%), no substantial quenching was observed when compared to the analogous non-injecting sample with insulating Al_2O_3. This suggest a short charge carrier diffusion length,[60,67] and that not all carriers are able to reach the quenching TiO_2. Even when exciting through the glass, which generates more of the photoexcited charge carriers closer to the perovskite/TiO_2 interface, there is still a long-lived tail suggesting that the electron injection is suboptimal and a number of electrons are not injected into the TiO_2. In contrast, the relative quenching in the overstoichiometric sample (+10%) is much more substantial. The difference between exciting the injecting sample from the top-side and the glass-side is much less, suggesting longer charge carrier diffusion lengths and improved electron injection. These results collectively suggest that devices with the understoichiometric (−10%) composition would have more limited J_{sc} than the overstoichiometric configurations.

Discussion and Device Performance. A large number of complete devices were made with compositions ranging from PbI_2-deficient, or understoichiometric, (−10%) to PbI_2-rich, or overstoichiometric, (+30%). The device architecture and the physical appearance are given in Figure 9a−c. The power conversion efficiencies vary over a broad range. The best cells had efficiencies above 18% (Figure 9d), whereas the worse compositions gave cells close to 10%.

To focus on the specific effect on PbI_2 and to get a clearer parameter window, we were, as elaborated in the Experimental Methods section, using compositions slightly different from the optimized ones giving top efficiencies above 20%.[20] The compositions used here are close enough and 18% efficiency is high

DOI: 10.1021/jacs.6b06320
J. Am. Chem. Soc. 2016, 138, 10331−10343

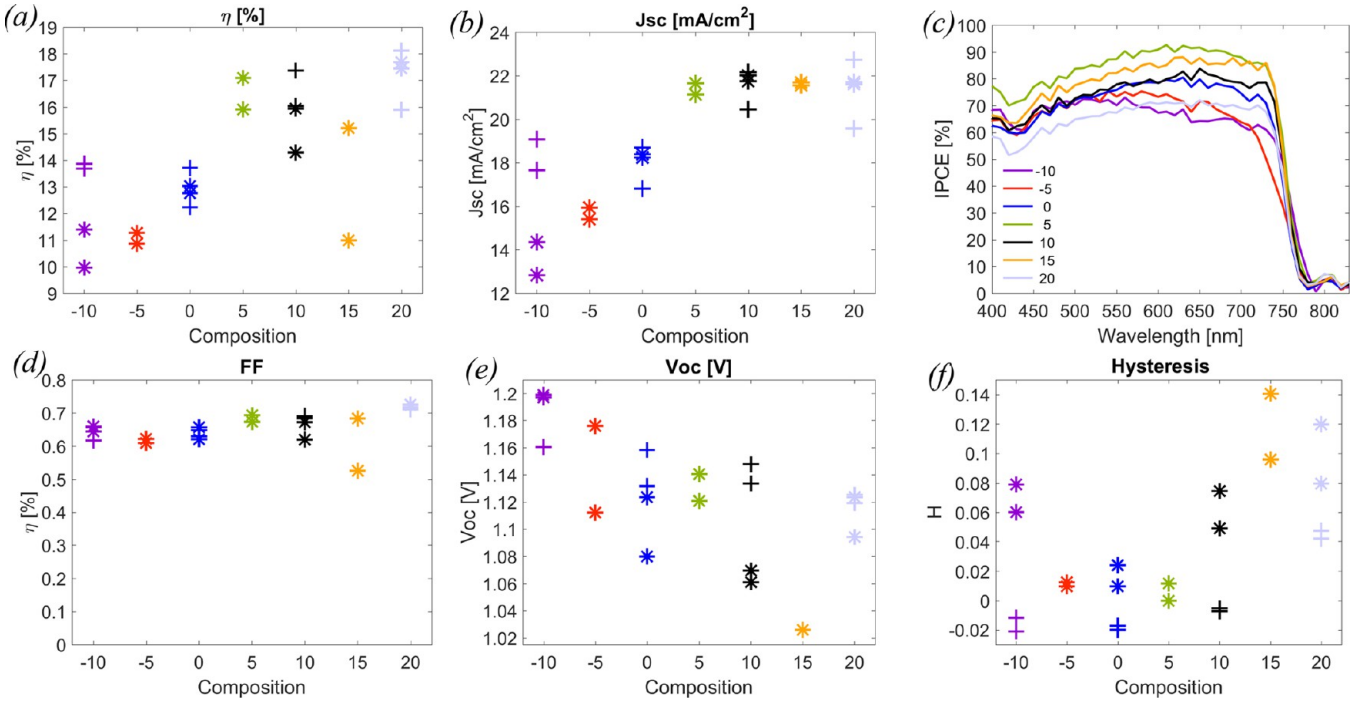

Figure 10. (a) η against stoichiometry. (b) J_{sc} (c) EQE against wavelength. (d) FF. (e) V_{oc}. (f) Hysteresis index H. The complete set of JV curves for all individual samples and the corresponding data in tabular format are found in the SI.

enough for the physics explored here to be generalizable to the highest performing devices.

The cell efficiencies decreased for the more PbI_2-deficient samples (Figure 10a), which is in line with previous reports.[19,21,26] The drop in efficiency was mainly a consequence of decreased photocurrents (Figure 10b). Those are robust observations reproduced in all batches made. On the basis of the PL data (Figure 8), the decrease in J_{sc} is probably an effect of poor charge transport in the understoichiometric samples, possibly caused by an enrichment of organic species in the grain boundaries. The PES, XRD, UV−vis and PL measurements together with mass balance constraints indicates that the grain boundaries get enriched in organic species in the understoichiometric samples. Band diagram computations predict that the organic ions not contribute with states close to the band edges.[50,68] Transport of photoexcited thermalized charge carriers is thus mainly occurring in bands originating from the lead halide framework. PbI_2-deficient conditions result in a disruption of that framework by enriching the grain boundaries with organic ions. The grain boundaries could then act as barriers toward charge transport, explaining the lower photocurrents. The XRD measurements indicate that grains in the understoichiometric samples may be polycrystalline, which also would increase the number of internal grain boundaries the charge carriers would need to pass in order to be collected.

External quantum efficiency (EQE) measurements show that for higher photon energies, the collection is independent of stoichiometry (Figure 10c). For the understoichiometric samples, lower values are observed for photon energies ranging from the absorption onset up to approximately 2.25 eV. That correlates with the drop in photocurrent and could potentially be a result of trapping of low energy photocarriers close to the band edges, or to the shorter diffusion length and the inferior electron injection indicated in Figure 8.

The fill factor is essentially independent of stoichiometry (Figure 10d). The V_{oc} does, however, tend to decrease when the amount of PbI_2 increases (Figure 10e). The highest measured V_{oc} was as high as 1.20 V and found in one of the PbI_2-deficient samples. 1.20 V is remarkably high and close to what could be hoped for given a band gap of 1.64 eV. PbI_2 may thus be involved in two counterbalancing effects. Even if the device performance is better for PbI_2-rich devices, the excess PbI_2 may have a negative impact in decreasing the photovoltage. This balance may not always tip in the same direction, which would explain contradictory results in other reports,[18,19,21] as well as why this effect was not reproduced in every single batch. We should also point out that we have measured high, even though not equally high, V_{oc} values for overstoichiometric samples (1.17 V with a mesoporpus TiO_2 architecture and 1.19 with a planar SnO_2 electron selective contact). Still, the higest V_{oc} measured in the group for the mixed perovskite is for the PbI_2-deficient samples here discussed, and high V_{oc} values for PbI_2-deficient cells were reproduced in most, even if not in all, batches.

To verify whether the high open-circuit voltage correlates with high luminescence efficiencies, as expected from fundamental theory, electroluminescence was measured on devices with different stoichiometry. This was indeed the case, even though we observed measurement related variations, possibly due to a reversible instability related to hysteresis and degradation under long time storage before the measurements. The highest value of the external electroluminescence quantum efficiency (EQE_{EL}) in this series was measured for a −5% device and approached 0.8% at a current of 20 mA/cm^2 (SI). This is in good agreement with a V_{oc} of 1.20 V[19,69] and is as far as we know a record value. The EQE_{EL} increases approximately linearly with driving current as expected for a trap-recombination limited current[70] (SI).

The high V_{oc} for the PbI_2-poor devices are also in good agreement with the longer lifetimes demonstrated in Figure 8. These high V_{oc} values may be explained by higher crystal quality in the PbI_2-poor devices. The higher PL intensities and the high EQE_{EL} supports that claim. The TEM data (Figure 6), which

DOI: 10.1021/jacs.6b06320
J. Am. Chem. Soc. 2016, 138, 10331−10343

indicate more small PbI_2-inclusions within the perovskite grains in the PbI_2-rich samples support this as well.

The dynamics of the crystallization and formation of the perovskite phase may be able to give a rationalization behind these observations. The perovskite formation is likely initiated by PbI_2 crystallization followed by perovskite formation by diffusion of the organic ions into the PbI_2 structure. For two-step protocols this is trivially true, but it seems to be the case also for the one-step protocol. This is supported by the PES data, which indicate a surplus of organic salts on the surface also for PbI_2-deficient stoichiometries. In this mode of growth, the simple concept of chemical equilibria implies that PbI_2-rich conditions will result in noncomplete conversion of the PbI_2-grains, which thus will contain inclusions of unreacted PbI_2 (as seen in TEM section), which due to strain will be amorphous (as given by the peak width in XRD). As the highest performing devices are PbI_2-rich, these PbI_2 inclusions are obviously not detrimental. A surplus of organic ions, as fond under PbI_2-deficient conditions, could shift the equilibrium toward more complete conversion of PbI_2 and thus generate a more homogeneous and pure perovskite phase. Taken on its own, that would be intrinsically better, as indicated by the PL and EQE_{EL} data. The downside is that the grain boundaries get enriched in organic species, as indicated by the PES data and a simple mass balance argument. That in turn correlates with shorter charge carrier diffusion length and slower injection into the back contact (Figure 8g,h) as well as a decrease in the EQE for lower photon energies (Figure 10c); both of which decreases the photocurrent (Figure 10b).

There is a hysteresis in the IV-curves (Figure 9d and SI). This have been widely observed and discussed,[71−74] and hypotheses for its origin involve ion migration,[75,76] interfacial charge transfer,[77] capacitive effects,[72] and ferroelectric effects.[78] A hysteresis index, H, is defined in eq 1, where J_b and J_f is the current in the backward and forward scan, respectively.

$$H = \frac{\int_0^{V_{oc}} J_b(V)\,dV - \int_0^{V_{oc}} J_f(V)\,dV}{\int_0^{V_{oc}} J_b(V)\,dV} \quad (1)$$

The hysteresis was generally higher in the PbI_2-rich samples (Figure 10f), whereas it was rather small in the stoichiometric and in most of the PbI_2-deficient samples. Our data suggests that difference in ion migration of the grain boundaries are the cause behind this trend. The grain boundaries in the PbI_2-deficient samples have, as discussed above, a higher organic content, that possible is more amorphous. The activation energy for ion migration is likely higher over those grain boundaries compared to more PbI_2-rich grain boundaries. Those grain boundaries would not have the same layered structure as crystalline PbI_2 where ion migration could occur between the layers in much the same way as the organic ions intercalate the PbI_2 structure during perovskite formation. If ion migration is the main cause of the hysteresis, which goes toward being the dominating hypothesis,[76,79] it would reasonably be smaller if the ions to a larger degree would be confined within individual grains.

This hypothesis is supported by PL measurements performed as a function of time under illumination.[54,55,80] We have performed a number of such measurements, which briefly are reproduced in the SI. We generally observe PL enhancements due to a reduction in nonradiative decay pathways and we recently reported that these PL enhancements are associated with a photoinduced migration of iodide-55. We find that this effect is most evident in the overstoichiometric samples, which are likely to have the highest excess of iodide, and this is consistent with this configuration showing the most exaggerated hysteresis effects. In contrast, the effects are greatly reduced in the stoichiometric and understoichiometric samples, which have less excess iodide and hysteresis effects. A broadening of the emission was also observed, which indicate the onset of a phase separation into more bromide and iodide rich phases. This effect was considerably more pronounced in the PbI_2-rich samples, consistent with lower barriers for ion migration and a higher hysteresis. From previous experiments,[20] we know that this type of phase separation can be detrimental for device performance. The stoichiometry is thus expected to affect also the stability, which will be further investigated.

SUMMARY AND CONCLUSIONS

We have used a broad range of techniques to investigate how the amount of remnant PbI_2 influences the properties of perovskite films and solar cells. We found the amount of PbI_2 to have a small or negligible effect on the phase composition and the surface morphology. The effect on the grain boundaries and the crystal quality was significant and had consequences for the charge carrier lifetimes, ion migration, photo luminescence, charge carrier injection, hysteresis, as well as on the device performance.

The highest device performance was, in line with previous results, obtained with PbI_2-rich samples and devices with efficiencies over 18% were produced. For PbI_2-deficient perovskites, the photocurrent and consequently also the device performance dropped. This was attributed to an accumulation of organic species in the grain boundaries, which were found to hinder the charge carrier transport and decrease the electron injection into the back contact. The PbI_2-deficient stoichiometries did, however, also have advantages. The highest V_{oc} were found for understoichiometric samples, and values as high as 1.20 V were measured. This could be correlated with high crystal quality, longer charge carrier lifetimes, and high PL and EQE_{EL} yields. On the basis of PES, TEM, XRD, SEM, and PL data, this could be rationalized as a consequence of the dynamics of the perovskite formation, which also for one-step protocols appears to be a two-step process where the perovskite is formed by intercalation of organic species in precipitated PbI_2-grains. A surplus of organic salts, i.e., a PbI_2-deficiency, leads to a more complete conversion of PbI_2 into the perovskite phase, which results in a more homogeneous perovskite phase of higher crystal quality. We also found the ion migration to be obstructed in the understoichiometric samples which decreased the JV hysteresis and increased the photostability.

One of the core conclusions is that PbI_2-deficient synthesis conditions can result in a perovskite phase with very high crystal quality, expressed in long lifetimes, and high PL and EQE_{EL} yields. The downside is grain boundaries enriched in organic species that provide a barrier toward current transport and decreases the photocurrent. An interesting prospect worth further investigations is to explore if the synthesis conditions can be tuned in such a way that the crystal quality here obtained under PbI_2-deficient conditions could be maintained while simultaneously generating grain boundaries with as favorable properties as under PbI_2-rich conditions. That could potentially be a way toward new record devices, and some work have been started along this direction.[81,82]

DOI: 10.1021/jacs.6b06320
J. Am. Chem. Soc. 2016, 138, 10331−10343

■ ASSOCIATED CONTENT

Supporting Information

The Supporting Information is available free of charge on the ACS Publications website at DOI: 10.1021/jacs.6b06320.

Details concerning synthesis, device production and characterization. Additional XRD, UV−vis, PL, SEM, PES, and valence band spectroscopy data. Band gap determinations. Full set of *JV*-figures and corresponding device data in tabular form. (PDF)

■ AUTHOR INFORMATION

Corresponding Authors

*jacobsson.jesper.work@gmail.com

*anders.hagfeldt@epfl.ch

Notes

The authors declare no competing financial interest.

■ ACKNOWLEDGMENTS

GRAPHENE project supported by the European Commission Seventh Framework Program under contract 604391 is gratefully acknowledged. BP and HR thank HZB for the allocation of synchrotron radiation beam time. SDS has received funding from the People Programme (Marie Curie Actions) of the European Union's Seventh Framework Programme (FP7/2007-2013) under REA grant agreement number PIOF-GA-2013-622630.

■ REFERENCES

(1) Kojima, A.; Teshima, K.; Shirai, Y.; Miyasaka, T. *J. Am. Chem. Soc.* **2009**, *131*, 6050.

(2) Im, J. H.; Lee, C. R.; Lee, J. W.; Park, S. W.; Park, N. G. *Nanoscale* **2011**, *3*, 4088.

(3) Lee, M. M.; Teuscher, J.; Miyasaka, T.; Murakami, T. N.; Snaith, H. J. *Science* **2012**, *338*, 643.

(4) Kim, H. S.; Lee, C. R.; Im, J. H.; Lee, K. B.; Moehl, T.; Marchioro, A.; Moon, S. J.; Humphry-Baker, R.; Yum, J. H.; Moser, J. E.; Gratzel, M.; Park, N. G. *Sci. Rep.* **2012**, *2*, 1.

(5) Heo, J. H.; Im, S. H.; Noh, J. H.; Mandal, T. N.; Lim, C. S.; Chang, J. A.; Lee, Y. H.; Kim, H. J.; Sarkar, A.; Nazeeruddin, M. K.; Gratzel, M.; Seok, S. I. *Nat. Photonics* **2013**, *7*, 487.

(6) Burschka, J.; Pellet, N.; Moon, S. J.; Humphry-Baker, R.; Gao, P.; Nazeeruddin, M. K.; Gratzel, M. *Nature* **2013**, *499*, 316.

(7) NREL efficiency chart.

(8) Snaith, H. J. *J. Phys. Chem. Lett.* **2013**, *4*, 3623.

(9) Bailie, C. D.; Christoforo, M. G.; Mailoa, J. P.; Bowring, A. R.; Unger, E. L.; Nguyen, W. H.; Burschka, J.; Pellet, N.; Lee, J. Z.; Graetzel, M.; Noufi, R.; Buonassisi, T.; Salleo, A.; McGehee, M. D. *Energy Environ. Sci.* **2015**, *8*, 956.

(10) Albrecht, S.; Saliba, M.; Baena, J. P. C.; Lang, F.; Kegelmann, L.; Mews, M.; Steier, L.; Abate, A.; Rappich, J.; Korte, L.; Schlatmann, R.; Nazeeruddin, M. K.; Hagfeldt, A.; Graetzel, M.; Rech, B. *Energy Environ. Sci.* **2016**, *9*, 81.

(11) Koh, T. M.; Fu, K.; Fang, Y.; Chen, S.; Sum, T. C.; Mathews, N.; Mhaisalkar, S. G.; Boix, P. P.; Baikie, T. *J. Phys. Chem. C* **2014**, *118*, 16458.

(12) Pellet, N.; Gao, P.; Gregori, G.; Yang, T.-Y.; Nazeeruddin, M. K.; Maier, J.; Graetzel, M. *Angew. Chem., Int. Ed.* **2014**, *53*, 3151.

(13) Lee, J.-W.; Seol, D.-J.; Cho, A.-N.; Park, N.-G. *Adv. Mater.* **2014**, *26*, 4991.

(14) Yang, W. S.; Noh, J. H.; Jeon, N. J.; Kim, Y. C.; Ryu, S.; Seo, J.; Seok, S. I. *Science* **2015**, *348*, 1234.

(15) Knop, O.; Wasylishen, R. E.; White, M. A.; Cameron, T. S.; Vanoort, M. J. M. *Can. J. Chem.* **1990**, *68*, 412.

(16) Heo, J. H.; Song, D. H.; Im, S. H. *Adv. Mater.* **2014**, *26*, 8179.

(17) Baena, J. P. C.; Steier, L.; Tress, W.; Saliba, M.; Neutzner, S.; Matsui, T.; Giordano, F.; Jacobsson, T. J.; Kandada, A. R. S.; Zakeeruddin, S. M.; Petrozza, A.; Abate, A.; Nazeeruddin, M. K.; Graetzel, M.; Hagfeldt, A. *Energy Environ. Sci.* **2015**, *8*, 2928.

(18) Jeon, N. J.; Noh, J. H.; Yang, W. S.; Kim, Y. C.; Ryu, S.; Seo, J.; Seok, S. I. *Nature* **2015**, *517*, 476.

(19) Bi, D.; Tress, W.; Dar, M. I.; Gao, P.; Luo, J.; Renevier, C.; Schenk, K.; Abate, A.; Giordano, F.; Correa Baena, J.-P.; Decoppet, J.-D.; Zakeeruddin, S. M.; Nazeeruddin, M. K.; Grätzel, M.; Hagfeldt, A. *Sci. Adv.* **2016**, *2*, e1501170.

(20) Jesper Jacobsson, T.; Correa-Baena, J.-P.; Pazoki, M.; Saliba, M.; Schenk, K.; Gratzel, M.; Hagfeldt, A. *Energy Environ. Sci.* **2016**, *9*, 1706.

(21) Roldan-Carmona, C.; Gratia, P.; Zimmermann, I.; Grancini, G.; Gao, P.; Graetzel, M.; Nazeeruddin, M. K. *Energy Environ. Sci.* **2015**, *8*, 3550.

(22) Kim, Y. C.; Jeon, N. J.; Noh, J. H.; Yang, W. S.; Seo, J.; Yun, J. S.; Ho-Baillie, A.; Huang, S.; Green, M. A.; Seidel, J.; Ahn, T. K.; Il Seok, S. *Adv. Energ. Mater.* **2016**, *6*, 1502104.

(23) Burschka, J.; Pellet, N.; Moon, S.-J.; Humphry-Baker, R.; Gao, P.; Nazeeruddin, M. K.; Graetzel, M. *Nature* **2013**, *499*, 316.

(24) Chen, Q.; Zhou, H.; Hong, Z.; Luo, S.; Duan, H.-S.; Wang, H.-H.; Liu, Y.; Li, G.; Yang, Y. *J. Am. Chem. Soc.* **2014**, *136*, 622.

(25) Lee, Y. H.; Luo, J.; Humphry-Baker, R.; Gao, P.; Graetzel, M.; Nazeeruddin, M. K. *Adv. Funct. Mater.* **2015**, *25*, 3925.

(26) Cao, D. H.; Stoumpos, C. C.; Malliakas, C. D.; Katz, M. J.; Farha, O. K.; Hupp, J. T.; Kanatzidis, M. G. *APL Mater.* **2014**, *2*, 091101.

(27) Bi, D.; El-Zohry, A. M.; Hagfeldt, A.; Boschloo, G. *ACS Photonics* **2015**, *2*, 589.

(28) Supasai, T.; Rujisamphan, N.; Ullrich, K.; Chemseddine, A.; Dittrich, T. *Appl. Phys. Lett.* **2013**, *103*, 183906.

(29) Chen, Q.; Zhou, H.; Song, T.-B.; Luo, S.; Hong, Z.; Duan, H.-S.; Dou, L.; Liu, Y.; Yang, Y. *Nano Lett.* **2014**, *14*, 4158.

(30) Wang, S.; Dong, W.; Fang, X.; Zhang, Q.; Zhou, S.; Deng, Z.; Tao, R.; Shao, J.; Xia, R.; Song, C.; Hu, L.; Zhu, J. *Nanoscale* **2016**, *8*, 6600.

(31) Salim, T.; Sun, S.; Abe, Y.; Krishna, A.; Grimsdale, A. C.; Lam, Y. M. *J. Mater. Chem. A* **2015**, *3*, 8943.

(32) Shao, Y.; Xiao, Z.; Bi, C.; Yuan, Y.; Huang, J. *Nat. Commun.* **2014**, *5*, 5784.

(33) Nakayashiki, S.; Daisuke, H.; Ogomi, Y.; Hayase, S. *J. Photonics Energy* **2015**, *5*, 057410.

(34) Somsongkul, V.; Lang, F.; Jeong, A. R.; Rusu, M.; Arunchaiya, M.; Dittrich, T. *Phys. Status Solidi RRL* **2014**, *8*, 763.

(35) Calloni, A.; Abate, A.; Bussetti, G.; Berti, G.; Yivlialin, R.; Ciccacci, F.; Duo, L. *J. Phys. Chem. C* **2015**, *119*, 21329.

(36) Wang, L.; McCleese, C.; Kovalsky, A.; Zhao, Y.; Burda, C. *J. Am. Chem. Soc.* **2014**, *136*, 12205.

(37) Haruyama, J.; Sodeyama, K.; Han, L.; Tateyama, Y. *J. Phys. Chem. Lett.* **2014**, *5*, 2903.

(38) Buin, A.; Pietsch, P.; Xu, J.; Voznyy, O.; Ip, A. H.; Comin, R.; Sargent, E. H. *Nano Lett.* **2014**, *14*, 6281.

(39) Yin, W.-J.; Shi, T.; Yan, Y. *Adv. Mater.* **2014**, *26*, 4653.

(40) Yun, J. S.; Ho-Baillie, A.; Huang, S.; Woo, S. H.; Heo, Y.; Seidel, J.; Huang, F.; Cheng, Y.-B.; Green, M. A. *J. Phys. Chem. Lett.* **2015**, *6*, 875.

(41) Jacobsson, T. J.; Tress, W.; Correa-Baena, J.-P.; Edvinsson, T.; Hagfeldt, A. *J. Phys. Chem. C* **2016**, *120*, 11382.

(42) Guerrero, A.; Garcia-Belmonte, G.; Mora-Sero, I.; Bisquert, J.; Kang, Y. S.; Jacobsson, T. J.; Correa-Baena, J.-P.; Hagfeldt, A. *J. Phys. Chem. C* **2016**, *120*, 8023.

(43) Correa-Baena, J.-P.; Anaya, M.; Lozano, G.; Tress, W.; Domanski, K.; Saliba, M.; Matsui, T.; Jacobsson, T. J.; Calvo, M. E.; Abate, A.; Grätzel, M.; Míguez, H.; Hagfeldt, A. *Adv. Mater.* **2016**, *28*, 5031.

(44) Giordano, F.; Abate, A.; Correa Baena, J. P.; Saliba, M.; Matsui, T.; Im, S. H.; Zakeeruddin, S. M.; Nazeeruddin, M. K.; Hagfeldt, A.; Graetzel, M. *Nat. Commun.* **2016**, *7*, 10379.

(45) Jacobsson, T. J.; Schwan, L. J.; Ottosson, M.; Hagfeldt, A.; Edvinsson, T. *Inorg. Chem.* **2015**, *54*, 10678.

(46) Zhao, Y.; Zhu, K. *J. Phys. Chem. Lett.* **2014**, *5*, 4175.

(47) Jeon, N. J.; Noh, J. H.; Kim, Y. C.; Yang, W. S.; Ryu, S.; Il Seol, S. *Nat. Mater.* **2014**, *13*, 897.

(48) Abate, A.; Leijtens, T.; Pathak, S.; Teuscher, J.; Avolio, R.; Errico, M. E.; Kirkpatrik, J.; Ball, J. M.; Docampo, P.; McPherson, I.; Snaith, H. J. *Phys. Chem. Chem. Phys.* **2013**, *15*, 2572.
(49) Abate, A.; Staff, D. R.; Hollman, D. J.; Snaith, H. J.; Walker, A. B. *Phys. Chem. Chem. Phys.* **2014**, *16*, 1132.
(50) Jacobsson, T. J.; Pazoki, M.; Hagfeldt, A.; Edvinsson, T. *J. Phys. Chem. C* **2015**, *119*, 25673.
(51) Jacobsson, T. J.; Edvinsson, T. *J. Phys. Chem. C* **2012**, *116*, 15692.
(52) Fondell, M.; Jacobsson, T. J.; Boman, M.; Edvinsson, T. *J. Mater. Chem. A* **2014**, *2*, 3352.
(53) Jacobsson, T. J.; Edvinsson, T. *J. Phys. Chem. C* **2014**, *118*, 12061.
(54) Tian, Y.; Peter, M.; Unger, E.; Abdellah, M.; Zheng, K.; Pullerits, T.; Yartsev, A.; Sundstrom, V.; Scheblykin, I. G. *Phys. Chem. Chem. Phys.* **2015**, *17*, 24978.
(55) Dequilettes, D. W.; Zhang, W.; Burlakov, V. M.; Graham, D. J.; Leijtens, T.; Osherov, A.; Bulovic, V.; Snaith, H. J.; Ginger, D. S.; Stranks, S. D. *Nat. Commun.* **2016**, *7*, 1.
(56) Li, G.; Ching, K. L.; Ho, J. Y. L.; Wong, M.; Kwok, H.-S. *Adv. Energ. Mater.* **2015**, *5*, 1401775.
(57) Philippe, B.; Park, B.-W.; Lindblad, R.; Oscarsson, J.; Ahmadi, S.; Johansson, E. M. J.; Rensmo, H. *Chem. Mater.* **2015**, *27*, 1720.
(58) Tanuma, S.; Powell, C. J.; Penn, D. R. *Surf. Interface Anal.* **1994**, *21*, 165.
(59) Kim, H.-S.; Lee, C.-R.; Im, J.-H.; Lee, K.-B.; Moehl, T.; Marchioro, A.; Moon, S.-J.; Humphry-Baker, R.; Yum, J.-H.; Moser, J. E.; Graetzel, M.; Park, N.-G. *Sci. Rep.* **2012**, DOI: 10.1038/srep00591.
(60) Xing, G.; Mathews, N.; Sun, S.; Lim, S. S.; Lam, Y. M.; Graetzel, M.; Mhaisalkar, S.; Sum, T. C. *Science* **2013**, *342*, 344.
(61) Manser, J. S.; Reid, B.; Kamat, P. V. *J. Phys. Chem. C* **2015**, *119*, 17065.
(62) Stamplecoskie, K. G.; Manser, J. S.; Kamat, P. V. *Energy Environ. Sci.* **2015**, *8*, 208.
(63) Filip, M. R.; Eperon, G. E.; Snaith, H. J.; Giustino, F. *Nat. Commun.* **2014**, *5*, 1.
(64) Geng, W.; Zhang, L.; Zhang, Y.-N.; Lau, W.-M.; Liu, L.-M. *J. Phys. Chem. C* **2014**, *118*, 19565.
(65) Quarti, C.; Mosconi, E.; Ball, J. M.; D'Innocenzo, V.; Tao, C.; Pathak, S.; Snaith, H. J.; Petrozza, A.; De Angelis, F. *Energy Environ. Sci.* **2016**, *9*, 155.
(66) Miller, O. D.; Yablonovitch, E.; Kurtz, S. R. *IEEE. J. Photovolt.* **2012**, *2*, 303.
(67) Stranks, S. D.; Eperon, G. E.; Grancini, G.; Menelaou, C.; Alcocer, M. J. P.; Leijtens, T.; Herz, L. M.; Petrozza, A.; Snaith, H. J. *Science* **2013**, *342*, 341.
(68) Pazoki, M.; Jacobsson, T. J.; Hagfeldt, A.; Boschloo, G.; Edvinsson, T. *Phys. Rev. B: Condens. Matter Mater. Phys.* **2016**, *93*, 4105.
(69) Tress, W.; Marinova, N.; Inganas, O.; Nazeeruddin, M. K.; Zakeeruddin, S. M.; Graetzel, M. *Adv. Energ. Mater.* **2015**, *5*, 1400812.
(70) Marinova, N.; Tress, W.; Humphry-Baker, R.; Dar, M. I.; Bojinov, V.; Zakeeruddin, S. M.; Nazeeruddin, M. K.; Gratzel, M. *ACS Nano* **2015**, *9*, 4200.
(71) Sanchez, R. S.; Gonzalez-Pedro, V.; Lee, J.-W.; Park, N.-G.; Kang, Y. S.; Mora-Sero, I.; Bisquert, J. *J. Phys. Chem. Lett.* **2014**, *5*, 2357.
(72) Kim, H.-S.; Park, N.-G. *J. Phys. Chem. Lett.* **2014**, *5*, 2927.
(73) Snaith, H. J.; Abate, A.; Ball, J. M.; Eperon, G. E.; Leijtens, T.; Noel, N. K.; Stranks, S. D.; Wang, J. T.-W.; Wojciechowski, K.; Zhang, W. *J. Phys. Chem. Lett.* **2014**, *5*, 1511.
(74) Unger, E. L.; Hoke, E. T.; Bailie, C. D.; Nguyen, W. H.; Bowring, A. R.; Heumueller, T.; Christoforo, M. G.; McGehee, M. D. *Energy Environ. Sci.* **2014**, *7*, 3690.
(75) Azpiroz, J. M.; Mosconi, E.; Bisquert, J.; De Angelis, F. *Energy Environ. Sci.* **2015**, *8*, 2118.
(76) Tress, W.; Marinova, N.; Moehl, T.; Zakeeruddin, S. M.; Nazeeruddin, M. K.; Gratzel, M. *Energy Environ. Sci.* **2015**, *8*, 995.
(77) Jena, A. K.; Chen, H.-W.; Kogo, A.; Sanehira, Y.; Ikegami, M.; Miyasaka, T. *ACS Appl. Mater. Interfaces* **2015**, *7*, 9817.
(78) Frost, J. M.; Butler, K. T.; Walsh, A. *APL Mater.* **2014**, *2*, 081506.
(79) Meloni, S.; Moehl, T.; Tress, W.; Franckevicius, M.; Saliba, M.; Lee, Y. H.; Gao, P.; Nazeeruddin, M. K.; Zakeeruddin, S. M.; Rothlisberger, U.; Graetzel, M. *Nat. Commun.* **2016**, *7*, 10334.
(80) Hoke, E. T.; Slotcavage, D. J.; Dohner, E. R.; Bowring, A. R.; Karunadasa, H. I.; McGehee, M. D. *Chem. Sci.* **2015**, *6*, 613.
(81) Zhang, T.; Guo, N.; Li, G.; Qian, X.; Zhao, Y. *Nano Energy* **2016**, *26*, 50.
(82) Son, D.-Y.; Lee, J.-W.; Choi, Y. J.; Jang, I.-H.; Lee, S.; Yoo, P. J.; Shin, H.; Ahn, N.; Choi, M.; Kim, D.; Park, N.-G. *Nature Energy* **2016**, *1*, 16081.

DOI: 10.1021/jacs.6b06320
J. Am. Chem. Soc. 2016, 138, 10331−10343